J Solid State Electrochem (2012) 16:2071–2077
DOI 10.1007/s10008-011-1615-1

ORIGINAL PAPER

Performance of cathode-supported SOFC with $Ni_{0.5}Cu_{0.5}$–CGO anode operated in humidified hydrogen and in low-concentration dry methane

Gang Chen · Guoqing Guan · Yutaka Kasai · Hong-Xin You · Abuliti Abudula

Received: 7 August 2011 / Revised: 30 November 2011 / Accepted: 4 December 2011 / Published online: 21 December 2011
© Springer-Verlag 2011

Abstract A $Ni_{0.5}Cu_{0.5}$–CGO ($Ce_{0.8}Gd_{0.2}O_{1.9}$) anode in a LSM ($(La_{0.75}Sr_{0.25})_{0.95}MnO_{3-\delta}$)–CGO cathode-supported SOFC is tested in humidified H_2 (3% H_2O) and in low concentration of dry methane, respectively. After co-sintering at 1,300 °C, it was found that the A-site-deficient LSM effectively hindered the formation of $La_2Zr_2O_7$ or $SrZrO_3$. The OCVs of the cell are as high as 1.132, 1.14, and 1.147 V in humidified H_2 and 1.314, 1.269, and 1.2 V in 14.8% of dry methane at 850, 800 and 750 °C, respectively, indicating that the ScSZ electrolyte film prepared by the present method is dense enough. The corresponding peak power densities are 0.396, 0.287, and 0.19 Wcm^{-2} in humidified H_2 and 0.249, 0.164, and 0.096 Wcm^{-2} in 14.8% of dry methane at 850, 800, and 750 °C, respectively. The prepared cathode-supported SOFC with NiCu–CGO bimetallic anode shows long-term stability when dry methane is used as fuel.

Keywords Solid oxide fuel cell · Cathode-supported · Bimetallic anode · Methane

G. Chen (✉) · A. Abudula
Graduate School of Science and Technology, Hirosaki University,
1-Bunkyocho,
Hirosaki 036-8560, Japan
e-mail: chen_1721@hotmail.com

G. Guan · A. Abudula (✉)
North Japan Research Institute for Sustainable Energy (NJRISE),
Hirosaki University,
2-1-3, Matsubara,
Aomori 030-0813, Japan
e-mail: abuliti@cc.hirosaki-u.ac.jp

Y. Kasai
Aomori Prefectural Industrial Technology Research Center,
Industrial Research Institute,
4-11-6, Second Tonyamachi,
Aomori 030-0113, Japan

H.-X. You
Chemical Engineering College, Dalian University of Technology,
No. 2 Linggong Road,
Dalian 116024, People's Republic of China

Introduction

As a device that convert chemical energy into electric power through electrochemical reactions at elevated temperatures, solid oxide fuel cells (SOFC) have attracted increasing attention due to its high energy conversion efficiency, low emission, and flexibility of choices of fuels [1]. SOFC that operate directly with hydrocarbon fuels without external reforming is expected to become an important technology for power generation in the future [2, 3]. There are several disadvantages associated with traditional SOFC anode materials such as Ni/YSZ and these include Ni coarsening, sulfur poisoning, carbon deposition, and redox instability [4–6]. Recently, several alternative materials such as Cu–CeO_2 and ceramic materials have been developed as potential anodes [4, 7–10]. Compared to cermet ones, ceramic anodes are difficult to get sintered and can withstand sulfur contamination and carbon deposition even when they work for a long time. However, due to either low electrical conductivity or low electrochemical activity, their performance is still lower than that of the cermet anode [4, 11]. Therefore, Ni anode is still recognized as the most active material for the oxidation of hydrocarbon fuels. Gorte et al. [8–10] found that carbon deposition was avoided by using a Cu–CeO_2 anode. It is possible that Cu is a poor catalyst for forming and breaking C–C bonds and can hinder the formation of carbon on itself [11]. However, it is difficult to prepare Cu–YSZ cermets via high-temperature sintering technology

because the melting points of both copper (1,085 °C) [12] and copper oxide are significantly less than 1,500 °C, which is necessary for the densification of electrolytes. An approach for enhancing the activity and thermal stability of Cu-based anodes could be achieved by alloying the Cu with a more catalytically active metal with a higher melting temperature. Several authors [13, 14] demonstrated that carbon formation was greatly suppressed when Cu–Ni alloy-based anode was used instead of Ni-based anode. In addition, Kendall et al. [15] found that carbon deposition could also be suppressed if diluted methane was used to replace pure methane as fuel. In this case, low concentration of methane could be completely reacted with oxygen ions, and less carbon deposition could occur due to partial oxidation of methane (POM).

To date, four main types of SOFC structures, i.e., electrolyte-, anode-, cathode-, and metal-supported SOFC, have been studied [16]. The cathode-supportedtype shows various structural advantages over other varieties. In this type of SOFC, the anode and electrolyte can be very thin, and those problems such as oxygen transport in the anode, volume contraction, and expansion related to anode redox cycles and ionic resistance of the electrolyte can be avoided [1, 16, 17]. On the other hand, some novel anodes with low sintering temperature or low electronic conductivity for hydrocarbon fuels are easy to be used in cathode-supported SOFC. Furthermore, the possibility of applying low-cost cathode-supporting materials such as LSM has the advantage with regards to commercialization of SOFC [18]. However, in the preparation of cathode-supported SOFC, it was found that the formation of zirconate phases ($La_2Zr_2O_7$ and $SrZrO_3$) at the interface of the LSM and zirconia-based electrolyte resulted in the degradation of the cell [19]. In order to solve this problem, A-site-deficient materials such as $(La_{0.75}Sr_{0.25})_{0.95}MnO_{3-\delta}$, which showed less reactivity with a zirconia-based electrolyte compared with its stoichiometric counterpart even at high temperatures during the preparation stages, have been developed [1, 20].

In this study, NiCu–CGO anode was prepared on cathode-supported SOFC at low temperatures, and its electrochemical performance was evaluated in humidified hydrogen and in low concentration of dry methane, respectively. To significantly reduce the cost of fabrication, a thin 11 mol% Sc_2O_3-doped ZrO_2 (ScSZ) electrolyte film was prepared on a LSM–CGO cathode substrate via a cost-effective and simple dual-dry pressing method.

Experimental

Fabrication of unit cells

$Ni_{0.5}Cu_{0.5}O_x$ powder was prepared by a glycine-nitrate combustion method as reported previously [21]. Stoichiometric amounts of $Ni(NO_3)_2{\cdot}6H_2O$ and $Cu(NO_3)_2{\cdot}3H_2O$ were first mixed and dissolved in deionised water and glycine powder was then added to the solution at a molar ratio of metal ions to glycine of 1:0.75. The solution was heated and stirred on a hot plate at 70 °C to form a gel. The gel was subsequently heated on a hot plate until it ignited, producing a metal-oxide "ash". The ash was then heated to 650 °C to remove possible carbon residues, and finally a crystalline oxide powder was obtained. The starting materials for fabrication of the cathode were commercial A-site-deficient LSM (CAS, China), CGO (CAS, China), and starch powder in a weight ratio of 6:4:3.5. The assembly of LSM–CGO cathode substrate and ScSZ (Tosoh Corporation, Japan) electrolyte was prepared by a dual-dry pressing method [22]. In order to achieve higher bending strength of the cell using a sufficiently dense electrolyte film, the assembly was subsequently sintered at 1,300 °C for 8 h in air. $Ni_{0.5}Cu_{0.5}O_x$–CGO powder in a weight ratio of 6:4 was ball-milled in ethanol for 24 h and used for fabrication of the anode via a slurry coating method. This was followed by sintering at 1,000 °C in air for 3 h to form a porous anode. The effective area of the anode was 0.78 cm^2. To compare the long-term stability with $Ni_{0.5}Cu_{0.5}O_x$–CGO anode in low concentration of dry CH_4, NiO–CGO anode was also prepared on a cathode–electrolyte substrate by the same method with $Ni_{0.5}Cu_{0.5}O_x$–CGO anode and then sintered at 1,300 °C in air for 3 h. As-prepared cell was mounted in a test rig, in which glass ring was used to seal the cell. The cell performances were measured at different temperatures of 850, 800, and 750 °C by changing the external load in humidified H_2 (3% H_2O) and in low-concentration dry methane, respectively. The outlet gases of the anode were analyzed on-line with an Agilent GC 7890A gas chromatography system. A time of 10 min was allowed for each measurement for every change in current value imposed.

Measurement

The current collector was Pt mesh. The anode was reduced with hydrogen for 30 min. The flow rates of humidified H_2 and O_2 were both 100 ml min^{-1}. The flow rate of 14.8% of dry methane with Ar was kept at 54 ml min^{-1}. The impedances were measured between 0.1 Hz and 1 MHz using a frequency response analyzer and a potentiostat (Solartron 1255B and 1287, respectively) under open-circuit conditions. The microstructure and morphology of the cells after testing were characterized by scanning electron microscopy (SEM, Hitachi, S-800, Japan). To check the interface reaction between the ScSZ film and LSM–CGO cathode substrate during the preparation stage, ScSZ and LSM powder in a weight ratio of 1:1 was ball-milled in ethanol for 24 h, co-sintered at 1,250 and 1,350 °C, respectively, and the composite obtained was analyzed by X-

ray diffraction (XRD, Shimadazu, Japan) with Cu Kα radiation. The porosity of the cathode substrate was determined by the Archimedes method.

Results and discussion

The XRD patterns of (I) ScSZ–$La_{0.75}Sr_{0.25}MnO_3$ (stoichiometric LSM) and (II) ScSZ–$(La_{0.75}Sr_{0.25})_{0.95}MnO_{3-\delta}$ (A-site-deficient LSM) composite powders are shown in Fig. 1a. One can see that $La_2Zr_2O_7$ was formed in ScSZ and the stoichiometric LSM composite powder after sintering at 1,250 °C, but no $La_2Zr_2O_7$ or $SrZrO_3$ was found in ScSZ and A-site-deficient LSM composite powder even after sintering at 1,350 °C, confirming that the A-site-deficient LSM could effectively hinder the formation of $La_2Zr_2O_7$ or $SrZrO_3$, which could affect the performance of the SOFC. Figure 1b shows the XRD pattern of the

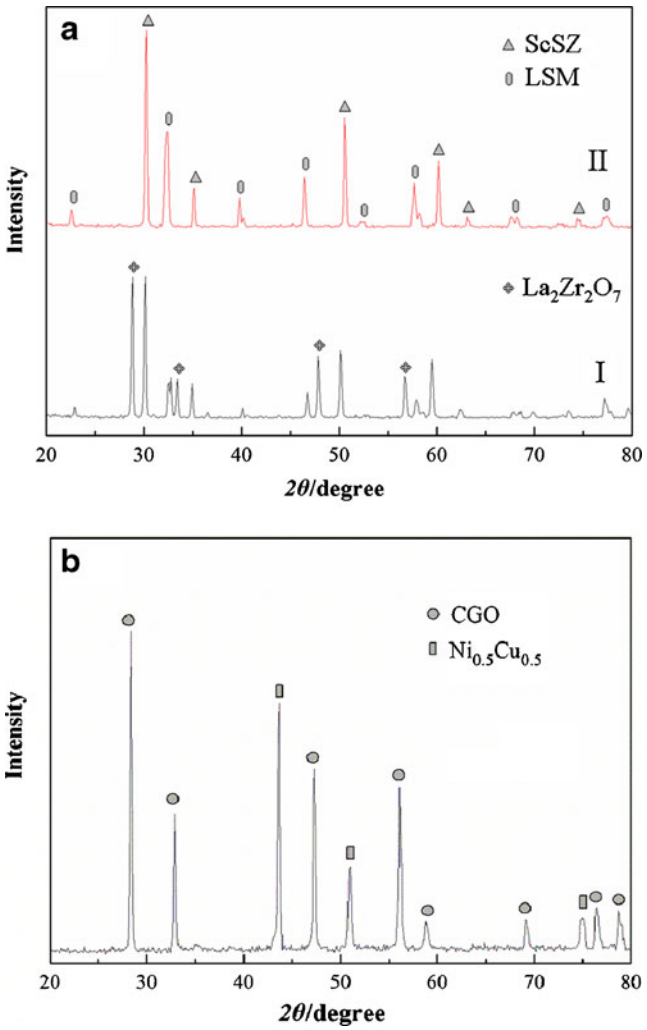

Fig. 1 **a** XRD patterns of (*I*) ScSZ+$La_{0.75}Sr_{0.25}MnO_3$ and (*II*) ScSZ+$(La_{0.75}Sr_{0.25})_{0.95}$ $MnO_{3-\delta}$ composite powders co-sintered at 1,250 and 1,350 °C, respectively. **b** XRD pattern of the $Ni_{0.5}Cu_{0.5}$–CGO cermet

$Ni_{0.5}Cu_{0.5}$–CGO cermet. In this case, the $Ni_{0.5}Cu_{0.5}$–CGO cermet was obtained by reducing the $Ni_{0.5}Cu_{0.5}O_x$–CGO pellet in H_2. One can see that a good $Ni_{0.5}Cu_{0.5}$ alloy was formed after reduction in hydrogen.

Figure 2 shows the cross-sectional SEM image of the sandwich structure of the whole cell (a) and the highly magnified morphology of the electrolyte (b). The thicknesses of the cathode substrate, anode, and electrolyte were approximately 680, 12, and 35 μm, respectively. Some isolated defects such as small voids could be observed in the electrolyte film. However, no cross-membrane cracks or pinholes were observed. The open-circuit voltages (OCVs) of the cell were 1.14 and 1.269 V at 800 °C in humidified H_2 and in 14.8% of dry methane, respectively, indicating that the ScSZ layer was sufficiently dense and could prohibit crossover of gases through the layer. As shown in Fig. 2a, the electrodes showed typical porous microstructures. The porosity of the cathode substrate was approximately 38%.

Figure 3 shows typical *I–V* curves of the as-prepared fuel cell at various temperatures in humidified H_2. The peak

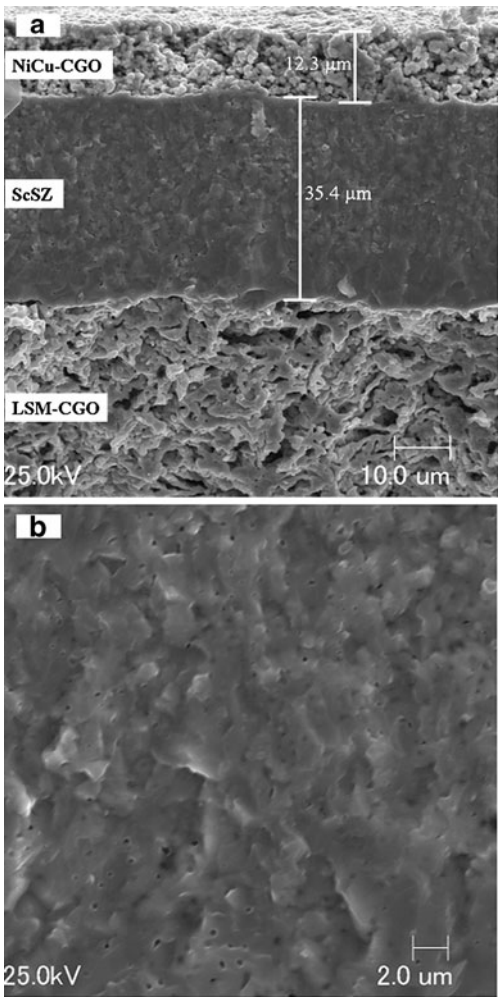

Fig. 2 **a** Cross-section of the sandwich structure of the whole cell. **b** High magnification of the electrolyte

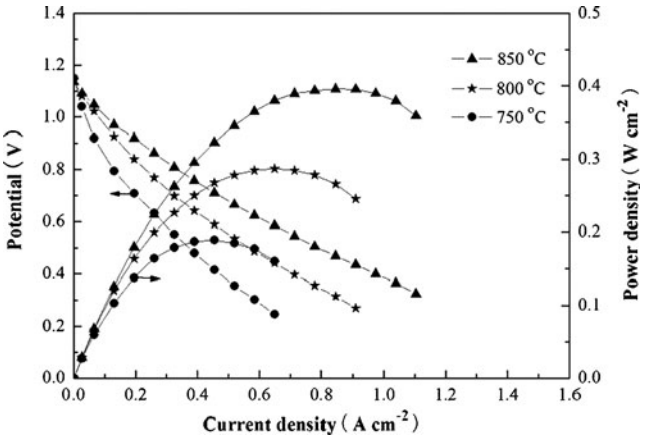

Fig. 3 Typical *I–V* curves of the cell at different temperatures in humidified H_2

power densities were 0.396, 0.287, and 0.19 W cm^{-2} at 850, 800, and 750 °C, respectively. The corresponding OCVs of the cell were 1.132, 1.14, and 1.147 V, respectively, which agree well with the theoretical values as predicted by the Nernst equation [23]. Furthermore, the power densities were a little higher than those of the tubular cathode-supported cell at the same temperatures [24], and this may be attributed to the much denser electrolyte film used in the present study.

Figure 4 shows typical *I–V* curves of the as-prepared fuel cell at different temperatures in 14.8% of dry methane. The OCVs of the cell were 1.314, 1.269, and 1.2 V at 850, 800, and 750 °C, respectively. The corresponding peak power densities were 0.249, 0.164, and 0.096 W cm^{-2}, respectively. The higher OCVs may be due to the partial oxidation of methane (POM) under open-circuit conditions [15]. The standard electromotive forces of POM calculated by the Nernst equation were 1.228 and 1.336 V at 800 and 900 °C, respectively [25]. The OCVs as well as the power densities of the $Ni_{0.5}Cu_{0.5}$–CGO bimetallic anode

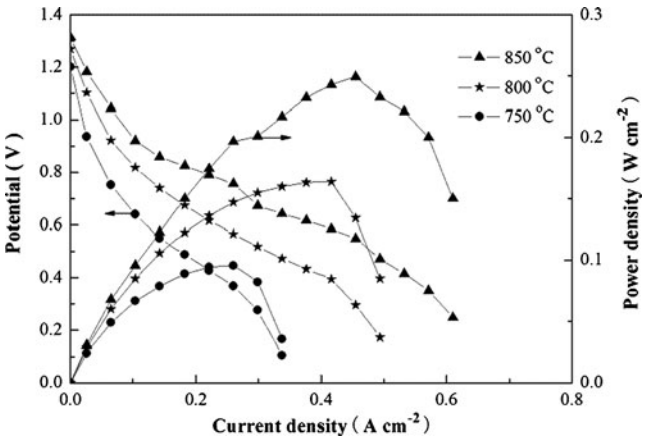

Fig. 4 Typical *I–V* curves of the cell at different temperatures in 14.8% of dry methane

in CH_4 fuel shown here were higher than those of CGO-impregnated $La_{0.75}Sr_{0.25}Cr_{0.5}Mn_{0.5}O_3$ anodes at the same temperatures [26], indicating that the $Ni_{0.5}Cu_{0.5}$ bimetallic anode is a more active material for the oxidation of methane. Figure 5 shows voltage and current curves of SOFCs with Ni–CGO anode and $Ni_{0.5}Cu_{0.5}$–CGO anode after 11 h of operation time in 14.8% of dry methane at 800 °C with the current density of 0.218 A cm^{-2}, respectively. One can see that the output voltage of Ni–CGO anode SOFC in 14.8% of dry CH_4 decreased gradually with the testing time, indicating that slow carbon deposition occurred on Ni–CGO anode. However, almost no degradation was observed in $Ni_{0.5}Cu_{0.5}$–CGO anode SOFC in 11 h of operation. It indicated that the $Ni_{0.5}Cu_{0.5}$–CGO bimetallic anode should be a good potential anode for directly using dry methane as fuel with better carbon deposition withstanding ability. Figure 6a, b shows the SEM micrographs for the surface microstructure of $Ni_{0.5}Cu_{0.5}$–CGO anode reduced in H_2 and after testing in 14.8% of dry CH_4 for 11 h, respectively. As indicated in Fig. 6b, no obvious carbon fibers could be observed after testing in 14.8% of dry CH_4 for 11 h, which indicate that $Ni_{0.5}Cu_{0.5}$–CGO bimetallic anode with low concentration of CH_4 could effectively suppress carbon deposition and generate high power density.

Figure 7 shows the production rates of anode outlet gases when the as-prepared fuel cell was operated in 14.8% of methane at 850 °C. As indicated above, the ScSZ layer is sufficiently dense to prohibit crossover of gases through the layer and the cell was well sealed. In such case, it should be noted that the rate of O^{2-} transfer from the cathode side to the anode side should be controlled by the current. The production rates of CO_2, CO, and $(CH_4)_{out}$ were calculated based on measurements obtained from the GC. The water generation rate and the H_2 production

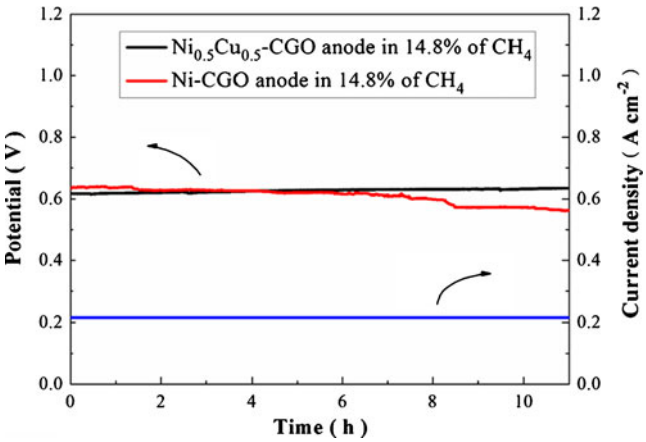

Fig. 5 Voltage and current curves of SOFCs with Ni–CGO anode and $Ni_{0.5}Cu_{0.5}$–CGO anode after 11 h operation time in 14.8% of dry methane at 800 °C, respectively, and the current density in each cell was maintained at 0.218 A cm^{-2}

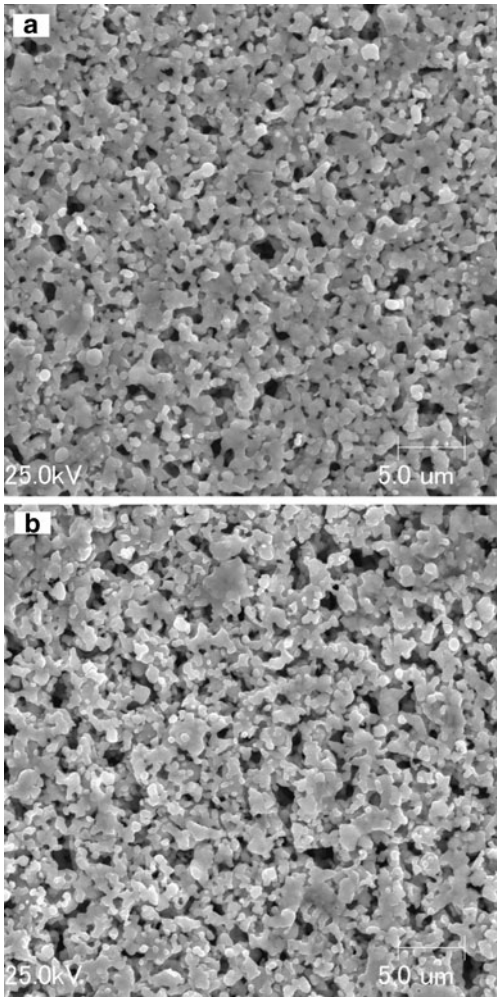

Fig. 6 SEM micrographs for the surface microstructure of $Ni_{0.5}Cu_{0.5}$–CGO anode reduced in humidified H_2 (**a**) and after testing in 14.8% of dry CH_4 for 11 h (**b**), respectively

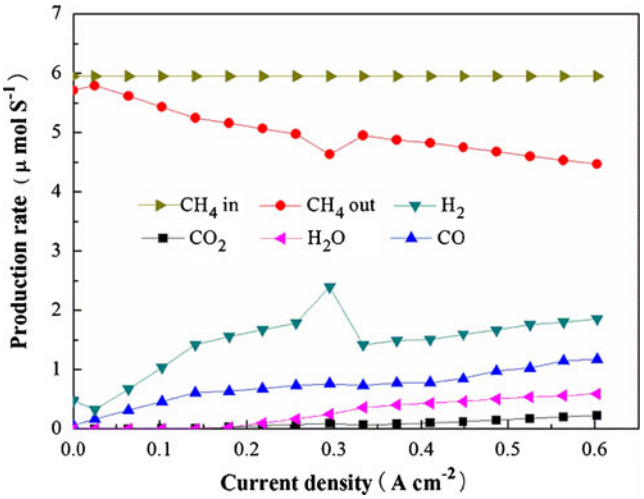

Fig. 7 Production rates of anodic exhausts from SOFC with 14.8% dry methane

rate were calculated in sequence via oxygen balance and hydrogen balance, respectively: [27]

$$v\left(O^{2-}\right) = I/2F \tag{1}$$

$$v(H_2O)_{fO} = v\left(O^{2-}\right) - v(CO)_{out} - 2v(CO_2)_{out} \tag{2}$$

$$v(H_2)_{fH} = 2\left[v(CH_4)_{in} - v(CH_4)_{out}\right] - v(H_2O)_{out} \tag{3}$$

where $v(CH_4)_{in}$ is the inlet flux of CH_4; $v(CH_4)_{out}$, $v(CO)_{out}$, $v(CO_2)_{out}$, and $v(H_2)_{fH}$ are the outlet fluxes of CH_4, CO, CO_2, and H_2, respectively. In Eq. 1, $v(O^{2-})$ is the O^{2-} flux calculated from the current (I) passing though the electrolyte and Faraday constant (F). As shown in Fig. 7, at a low current density with the open-circuit condition, the anode reaction mechanism was dominated by POM and methane cracking, and production rates of CO and H_2 increased with an increase in current density but no CO_2 and H_2O were generated. The POM dominated methane reactions at low-current densities. As the current increased (the amount of O^{2-} transported from cathode to anode increased), the production rate of H_2O increased. When current density increased above 0.256 A cm^{-2}, the production rates of H_2O and CO_2 both increased rapidly, indicating the start of complete oxidation of methane (COM). At the same current density, compared with POM ($CH_4+O^{2-}\rightarrow CO+2H_2+2e^-$), only fewer amounts of CH_4 could be consumed in the case of COM ($CH_4+ 4O^{2-}\rightarrow CO_2 +2H_2O+8e^-$). That is why the flux of CH_4 in outlet gases increased a little after the current density increased above 0.256 A cm^{-2}. To date, synthesis gas produced by partial oxidation of methane can be used as raw materials for the production of other chemicals. Therefore, co-producing synthesis gas through controlling methane reactions in the process of generating electricity attracts wide interest. As indicated in Fig. 7, the production rates of CO and H_2 were obviously higher than those of CO_2 and H_2O at each current density condition, indicating that NiCu alloy is also a good catalyst for generating synthesis gas while generating electricity.

Results of impedance spectroscopy carried out under open-circuit condition at different temperatures in humidified H_2 and in 14.8% of dry methane are shown in Fig. 8a, b, respectively. The high frequency intercept represents the ohmic resistance (R_o), which involves ionic resistance of the electrolyte, electronic resistance of the electrodes, and some contact resistances associated with interfaces. The difference between the high and low frequency intercepts represents the electrode polarization resistance (R_p) [23]. The R_o values of the cell are 0.45, 0.55, and 0.77 Ω cm^2 in humidified H_2 and 0.43, 0.56, and 0.78 Ω cm^2 in 14.8% of dry methane at 850, 800, and 750 °C, respectively. The R_p values of the cell in humidified H_2 are about 1.02, 1.92, and

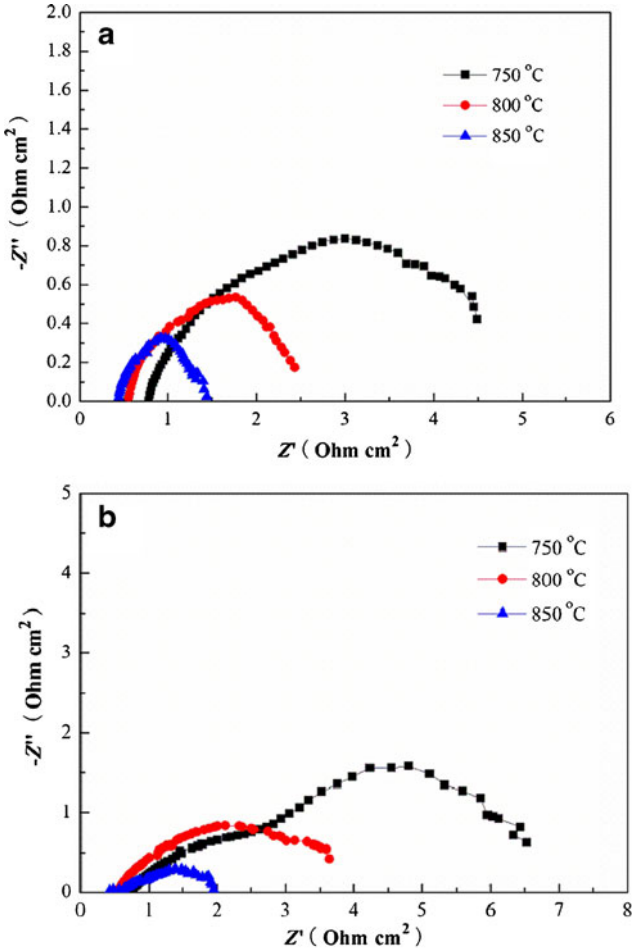

Fig. 8 Impedance spectra of the cathode-supported SOFC with NiCu–CGO anode in humidified H_2 (**a**) and in 14.8% dry methane (**b**) at various temperatures under open-circuit conditions

3.68 Ω cm^2 at 850, 800, and 750 °C, respectively, which are obviously smaller than those of the cell operated in 14.8% of dry methane at the same temperatures where the R_p values are about 1.52, 3.08, and 5.73 Ω cm^2, respectively. As shown in Fig. 7, only a small amount of CO appeared under the open-circuit condition. CO may be produced by the residual oxygen or by the O element from CGO or by the O^{2-} transported from the cathode as a small current which may have existed in the cells. This indicates that POM occurred at the $Ni_{0.5}Cu_{0.5}$–CGO anode under open-circuit in 14.8% of dry methane. Kendall et al. [15] also concluded that POM occurred in pure methane under open-circuit by comparing the experimental OCV with the theoretical OCV on Ni-based anodes. The higher R_p of the cell in 14.8% of dry methane indicates that the activation energy, E_a, of POM is higher than that of the hydrogen oxidation reaction at the $Ni_{0.5}Cu_{0.5}$–CGO anode. Similar results have been established for the Ni–YSZ anode. [28] The ionic conductivities of ScSZ were estimated to be 0.1 S cm^{-1} at 800 °C and 0.06 S cm^{-1} at 750 °C, respectively [29]. The corresponding ohmic resistances of the ScSZ electrolyte film were estimated to be 0.035 Ω cm^2 at 800 °C and 0.058 Ω cm^2 at 750 °C based on a ScSZ layer thickness of 35 μm and an electrode area of 0.78 cm^2, and they are much smaller than the experimental results of R_o at the same temperatures. The estimated electronic resistances of the NiCu–CGO anode and LSM–CGO cathode substrate should also be much smaller than the experimental results of R_o due to their higher electronic conductivity [30, 31]. In order to investigate the cathode–electrolyte interfacial resistance, a Pt anode was chosen to replace the NiCu–CGO anode, and in this case the electronic resistance of Pt and the contact resistance between Pt and electrolyte could be neglected. As shown in Fig. 9, the R_o of the cell with Pt anode was only a little lower than that of the cell with NiCu–CGO anode, indicating that the R_o in the cell with NiCu–CGO anode arose mainly from interfacial resistance between cathode and electrolyte. Yamaguchi et al. [32] indicated that the $(Zr,Ce)O_2$ phase, which has low ionic conductivity, could be formed at the interface of ScSZ and CGO at high sintering temperatures. Therefore, the high R_o in the cell with NiCu–CGO anode also could have resulted from the formation of $(Zr,Ce)O_2$ phase in this study. Yamaguchi et al. [32] also reported that the introduction of an activation layer between the cathode substrate and electrolyte reduced the electrode polarization significantly. Yamahara et al. [33] found that infiltration of Co into LSM–ScSZ cathode substrate enhanced the surface exchange of LSM and reduced electrode polarization. Thus, to avoid the interfacial reaction between ScSZ and CGO, reducing the sintering temperature of electrolyte film should be needed. In other words, to reduce the electrode polarization and improve the electrical performance of the present cathode-supported cell, optimization of the composition and microstructure of the cathode substrate is necessary.

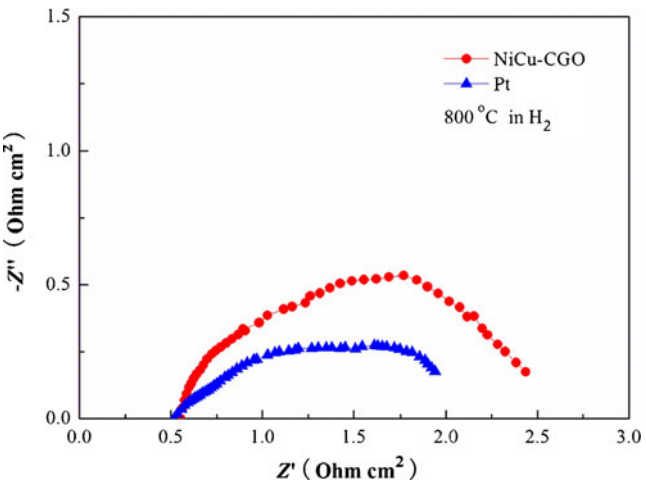

Fig. 9 Comparison of the impedance spectra of the cathode-supported SOFC with NiCu–CGO anode and Pt anode in humidified H_2 at 800 °C under open-circuit conditions

Conclusions

LSM–CGO cathode-supported SOFC were successfully fabricated by a cost-effective dual-drying pressing method. A-site-deficient LSM material was identified to be able to hinder the formation of impurities between the interfaces of LSM–CGO cathode and ScSZ electrolyte during the sintering process at 1,300 °C. $Ni_{0.5}Cu_{0.5}O_x$ alloy anode with good performance was prepared by a glycine-nitrate combustion method. High OCVs of the cell, i.e., 1.132, 1.14, and 1.147 V in humidified H_2 and 1.314, 1.269, and 1.2 V in 14.8% of dry methane at 850, 800, and 750 °C, respectively, were obtained, indicating that the as-prepared cell was well sealed and the ScSZ electrolyte film was sufficiently dense. The corresponding peak power densities reached 0.396, 0.287, and 0.19 Wcm^{-2} in humidified H_2 and 0.249, 0.164, and 0.096 Wcm^{-2} in 14.8% of dry methane at 850, 800, and 750 °C, respectively. An 11-h stability test indicated that NiCu–CGO could be used as a perspective anode for the direct use of dry methane as fuel. SEM morphologies indicated that cathode-supported SOFC with $Ni_{0.5}Cu_{0.5}$–CGO bimetallic anode could effectively suppress carbon deposition when a low concentration of methane was used as fuel.

Acknowledgements This study was supported by JSPS Grant-in-Aid for Scientific Research (11014675) and by the State Scholarship Fund of China Scholarship Council (2008).

References

1. Zhao C, Liu R, Wang S (2009) Electrochem Commun 11:842–845
2. Yoon S, Kim Y, Kim SY, Bae J (2010) J Solid State Electrochem 14:1793–1800
3. Li SL, Wang SR, Nie HW, Wen T-L (2006) J Solid State Electrochem 11:59–64
4. Atkinson A, Barnett S, Gorte RJ, Irvine JTS, Mcevoy AJ, Mogensen M, Singhal SC, Vohs JM (2004) Nat Mater 3:17–27
5. Lussier A, Sofie S, Dvorak J, Idzerd YU (2008) Int J Hydrogen Energy 33:3945–3951
6. Ettler M, Blab G, Menzler NH (2007) Fuel Cells 5:349–355
7. Tsipis EV, Kharton VV (2011) J Solid State Electrochem 15:1007–1040
8. Lu C, Worrell WL, Vohs JM, Gorte RJ (2003) J Electrochem Soc 150:A1357–A1359
9. Gorte RJ, Park S, Vohs JM, Wang CH (2000) Adv Mater 12:1465–1469
10. Raza MA, Rahman IZ, Beloshapkin S (2009) J Alloys Compd 485:593–597
11. Tao SW, Irvine JTS (2004) Chem Rec 4:83–95
12. Ye XF, Wang SR, Wang ZR, Xiong L, Sun XF, Wen TL (2008) J Power Sources 177:419–425
13. Kim H, Lu C, Worrell WL, Vohs JM, Gorte RJ (2002) J Electrochem Soc 149:A247–A250
14. Sin A, Kopnin E, Dubitsky Y, Zaopo A, Aricò AS, La Rosa D, Gullo LR, Antonucci V (2007) J Power Sources 164:300–305
15. Kendall K, Finnerty CM, Saunders G, Chung JT (2002) J Power Sources 106:323–327
16. Tucker MC (2010) J Power Sources 195:4570–4582
17. Sin A, Kopnin E, Dubitsky Y, Zaopo A, Aricò AS, Gullo LR, La Rosa D, Antonucci VJ (2005) J Power Sources 145:68–73
18. Ippommatsu M, Sasaki H, Otoshi S (1996) Int J Hydrogen Energy 21:129–135
19. Chervin C, Glass RS, Kauzlarich SM (2005) Solid State Ionics 176:17–23
20. Jiang SP (2008) J Mater Sci 43:6799–6833
21. Xie Z, Xia CR, Zhang MY, Zhu W, Wang HT (2006) J Power Sources 161:1056–1061
22. Chen G, You HX, Kasai Y, Sato H, Abudula A (2011) J Alloys Compd 509:5159–5162
23. McIntosh S, Vohs JM, Gorte RJ (2003) Electrochem Solid State Lett 6:A240–A243
24. Zhao CH, Liu R, Wang SR, Wang ZR, Qian JQ, Wen TL (2009) J Power Sources 192:552–555
25. Zhang X, Ohara S, Chen H, Fukui T (2002) Fuel 81:989–996
26. Chen XJ, Liu QL, Chan SH, Brandon NP, Khor KA (2007) Electrochem Commun 9:767–772
27. You HX, Gao HJ, Chen G, Abudula A, Ding XW (2011) J Power Sources 196:2779–2784
28. Hecht ES, Gupta GK, Zhu HY, Dean AM, Kee RJ, Maier L, Deutschmann O (2005) Appl Catal A Gen 295:40–51
29. Haering C, Roosen A, Schichl H, Schnfller M (2005) Solid State Ionics 176:261–268
30. Wang JX, Tao YK, Shao J, Wang WG (2009) J Power Sources 186:344–348
31. Zhu WZ, Deevi SC (2003) Mater Sci Eng A362:228–239
32. Yamaguchi T, Shimizu S, Suzuki T, Fujishiro Y, Awanoa M (2008) J Electrochem Soc 155:B423–B426
33. Yamahara K, Jacobson CP, Visco SJ, De Jonghe LC (2005) Solid State Ionics 176:451–456